Journal of Toxicology and Environmental Health, Part A: Current Issues
Publication details, including instructions for authors and subscription information:
http://www.tandfonline.com/loi/uteh20

Investigation of the Pulmonary Bioactivity of Double-Walled Carbon Nanotubes

Tina M. Sager [a], Michael W. Wolfarth [a], Lori A. Battelli [a], Stephen S. Leonard [a], Michael Andrew [a], Thomas Steinbach [b], Morinobu Endo [c], Shuji Tsuruoka [c], Dale W. Porter [a] & Vincent Castranova [a]

[a] National Institute for Occupational Safety and Health, Health Effects Laboratory Division, Pathology and Physiology Research Branch, Morgantown, West Virginia, USA

[b] Experimental Pathology Laboratories, Inc., Sterling, Virginia, USA

[c] Shinshu University, Research Center for Exotic Nanocarbons, Nagano, Japan

Published online: 24 Oct 2013.

To cite this article: Tina M. Sager, Michael W. Wolfarth, Lori A. Battelli, Stephen S. Leonard, Michael Andrew, Thomas Steinbach, Morinobu Endo, Shuji Tsuruoka, Dale W. Porter & Vincent Castranova (2013) Investigation of the Pulmonary Bioactivity of Double-Walled Carbon Nanotubes, Journal of Toxicology and Environmental Health, Part A: Current Issues, 76:15, 922-936, DOI: 10.1080/15287394.2013.825571

To link to this article: http://dx.doi.org/10.1080/15287394.2013.825571

Journal of Toxicology and Environmental Health, Part A, 76:922–936, 2013

ISSN: 1528-7394 print / 1087-2620 online
DOI: 10.1080/15287394.2013.825571

Taylor & Francis
Taylor & Francis Group

INVESTIGATION OF THE PULMONARY BIOACTIVITY OF DOUBLE-WALLED CARBON NANOTUBES

Tina M. Sager[1], Michael W. Wolfarth[1], Lori A. Battelli[1], Stephen S. Leonard[1], Michael Andrew[1], Thomas Steinbach[2], Morinobu Endo[3], Shuji Tsuruoka[3], Dale W. Porter[1], Vincent Castranova[1]

[1]National Institute for Occupational Safety and Health, Health Effects Laboratory Division, Pathology and Physiology Research Branch, Morgantown, West Virginia, USA
[2]Experimental Pathology Laboratories, Inc., Sterling, Virginia, USA
[3]Shinshu University, Research Center for Exotic Nanocarbons, Nagano, Japan

Double-walled carbon nanotubes (DWCNT) are a rather new and unexplored variety of carbon nanotubes. Previously conducted studies established that exposure to a variety of carbon nanotubes produced lung inflammation and fibrosis in mice after pharyngeal aspiration. However, the bioactivity of double-walled carbon nanotubes (DWCNT) has not been determined. In this study, the hypothesis that DWCNT would induce pulmonary toxicity was explored by analyzing the pulmonary bioactivity of DWCNT. To test this hypothesis, C57Bl/6 mice were exposed to DWCNT by pharyngeal aspiration. Mice underwent whole-lung lavage (WLL) to assess pulmonary inflammation and injury, and lung tissue was examined histologically for development of pulmonary disease as a function of dose and time. The results showed that DWCNT exposure produced a dose-dependent increase in WLL polymorphonuclear leukocytes (PMN), indicating that DWCNT exposure initiated pulmonary inflammation. DWCNT exposure also produced a dose-dependent rise in lactate dehydrogenase (LDH) activity, as well as albumin levels, in WLL fluid, indicating that DWCNT exposure promoted cytotoxicity as well as decreases in the integrity of the blood–gas barrier in the lung, respectively. In addition, at 7 and 56 d postexposure, the presence of significant alveolitis and fibrosis was noted in mice exposed to 40 μg/mouse DWCNT. In conclusion, this study provides insight into previously uninvestigated pulmonary bioactivity of DWCNT exposure. Data indicate that DWCNT exposure promotes inflammation, injury, and fibrosis in the lung.

Nanotechnology is currently at the forefront of scientific research and technological developments that resulted in the manufacture of novel consumer products and numerous industrial applications (Musee et al., 2011; Zhao and Castranova, 2011). Various nanomaterials have revolutionized many different industries, with emerging applications ranging from areas of biotechnology, electronics, and drug delivery, to cosmetics and sporting goods (Manke et al., 2012). Among the vastly expanding array of nanomaterials, carbon nanotubes (CNT) have received considerable attention from many investigators due to their interesting physicochemical properties and broad applications (Donaldson et al., 2010; Maynard et al., 2004).

Received 25 April 2013; accepted 12 July 2013.

The findings and conclusions in this report are those of the authors and do not necessarily represent the views of the National Institute for Occupational Safety and Health.

This work was supported in part by The Exotic Nanocarbon Project, Japan Regional Innovation Strategy Program for Excellence, JST. We thank Chemicals Research Laboratories, Toray Industries, Inc., for providing Toray DWCNT for this analysis. Also, we appreciate Robert Mercer, Sherri Friend, and Diane Schwegler-Berry for their excellent technical assistance with the enhanced dark-field and field emission scanning electron microcopy processes.

Address correspondence to Tina M. Sager, PhD, National Institute for Occupational Safety and Health, 1095 Willowdale Road, M/S 2015, Morgantown, WV 26505, USA. E-mail: sst2@cdc.gov

In addition to their outstanding mechanical characteristics, CNT exhibit reliable electrical and thermal properties. These superior properties provide exciting opportunities to produce advanced materials for new applications (Jorio et al., 2008; Abuilaiwi et al., 2010).

The structure of CNT facilitates their entry, deposition, and migration in the lungs and pleura, resulting in incomplete phagocytosis and clearance from the lungs (Stella, 2011). The biologically harmful effects believed to be induced by CNT are hypothesized to be due to their biopersistent and non-biodegradable nature, as well as their resemblance to needle-like asbestos fibers. In fact, CNT are similar to asbestos in their fibrous morphology, biopersistence, and ability to translocate from alveolar regions to the intrapleural space (Lam et al. 2004). Upon pulmonary exposure, CNT generate an acute inflammatory response, activate several cell signaling pathways, and induce genotoxicity, diffuse interstitial fibrosis, and granulomas in a manner similar to that observed in asbestos-exposed animals and humans (Jaurand et al., 2009; Tabet et al., 2009; Kim et al., 2010; Crouzier et al., 2010; Wang et al., 2010; Nagai et al., 2011).

Due to the rapid growth in the manufacturing and use of CNT, concerns have been raised about their potential adverse effects on both human health and the environment. It was postulated that human exposures to manufactured nanomaterials are most likely to be observed in workers rather than the general population (Bergamaschi, 2009). In fact, a recently published report estimated that approximately 6 million workers will be involved with the nanotechnology industry by 2020. Of these 6 million workers estimated to be working in the nanotechnology industry, one-third are predicted to reside in the United States (Patel, 2011).

As previously stated, due to their unique physical properties, carbon nanotubes (CNT) are at the forefront in the field of nanotechnology. There are three primary categories of CNT, single-walled (SWCNT), double-walled (DWCNT), and multiwalled (MWCNT), each possessing their own physical and chemical properties. For example, compared to SWCNT, DWCNT have a higher mechanical strength and thermal stability. DWCNT also possess interesting electronic and optical properties. In particular, the outer wall of the CNT can be functionalized (even covalently). Surface modification of DWCNT with functional moieties may play a key role in extending their applications in biological and industrial areas. The addition of surface functional groups to the CNT might alter the surface charge and reactivity of the surface, and enhance the stability and dispersion. For example, functionalization of a CNT with the COOH moiety changes the surface of the CNT from a hydrophobic state to hydrophilic state, thus providing active sites for further conjugation. Overall, these surface functionalizations/manipulations may be utilized to enhance dispersion, while maintaining reliable mechanical and electronic properties of the inner nanotube (Meunier et al., 2012).

Double-walled carbon nanotubes are an emerging class of carbon nanostructures and consist of two concentric CNT. This structure makes the DWCNT the simplest system for studying the effects of inner-wall coupling of the physical and bioactive properties of CNT (Shen et al., 2011). These DWCNT have received little commercial attention until recently, pending advances in the synthesis and separation of high-purity CNT samples. However, in vivo and in vitro studies investigating the bioactivity of DWCNT are lacking. Sager et al. (2013) and Porter et al. (2010) previously established that exposure to multiwalled carbon nanotubes (MWCNT) produced lung inflammation and fibrosis in mice after pharyngeal aspiration. However, as previously mentioned, the bioactivities of DWCNT have not been determined, and it is likely that DWCNT will differ from MWCNT due to differences in physicochemical properties (Table 1). Therefore, in this study, the hypothesis that DWCNT would promote pulmonary toxicity by analyzing the pulmonary responses to DWCNT exposure was examined.

TABLE 1. Characterization and Bioactivity Comparison of SWCNT, DWCNT, and MWCNT

		SWCNT	DWCNT	MWCNT
Charcterization	Manufacturer	Unidym Inc.	Toray Industries Inc.	West Virginia University
	Diameter (nm)	1–4 nm	1–2 nm	42 nm
	Length (μm)	1–3 μm	<5	0.76 μm
	Aspect ratio	750–1000	2500–5000	18.1
	Dose (μg/animal)	40 μg/mouse	1, 10, 40 μg/mouse	2.5, 10, 40 μg/mouse
		PBS	0.3% CMC	DM
Inflammatory response	PMN	Moderate (declined over 28 d)	Moderate/Persistent	Severe/Transient
	LDH	Moderate (stayed elevated over 28 d)	Moderate/Persistent	Severe/Transient
	Albumin	Not measured	Moderate/Persistent	Mild/Transient
Lung histpathology	Material in alveolar macrophages	Slight	All doses >Marked (d 7, 56)	All doses >Marked (d 7, 56)
	Material in TBL	N/A	40 μg Minimal (d 7) Mild (d 56)	40 μg Minimal (d 7) Mild (d 56)
	Alveolitis	Moderate at 28 days	>10 μg Moderate (d 7, 56)	Mild
	Fibrosis	Severe at 28 days	>10 μg Moderate (d 7, 56)	Mild

METHODS

DWCNT

DWCNT utilized in this study were obtained from Chemical Research Laboratories, Toray Industries, Inc., Nagoya, Japan. The DWCNT provided by Toray Industries were 1–2 nm in diameter and possessed a length less than 5 μm. The aspect ratio of the DWCNT is 2500–5000 (Table, 1).

DWCNT Trace Metal Analysis

To determine trace metals, bulk samples of the Toray DWCNT were first digested by a nitric/perchloric acid ashing procedure. Specifically, 4 ml concentrated nitric acid and 11 ml concentrated perchloric acid were added to each sample. The samples were then covered and refluxed at temperatures ranging from 150 to 180°C until complete dissolution had occurred (approximately 14 d). Next, the samples were heated to 140°C until they reached near-dryness. The remaining sample residues were then analyzed for trace metals by inductively coupled plasma–atomic emission spectroscopy (ICP-AES).

Electron Spin Resonance (ESR) Measurements

All electron spin resonance (ESR) measurements were conducted using a Bruker Instruments EMX ESR spectrometer and a flat cell assembly (Billerica, MA). Hyperfine couplings were measured (to 0.1G) directly from magnetic field separation using potassium tetraperoxochromate (K_3CrO_8) and 1,1-diphenyl-2-picrylhydrazyl (DPPH) as reference standards. Data acquisition and analysis were completed by the Acquisit Program (Billerica, MA). Each assay consisted of 100 m*M* hydrogen peroxide (H_2O_2) ± DWCNT (0.8 mg/ml) in a total volume of 1 ml carboxymethylcellulose (CMC) prepared in 0.9% NaCl. The H_2O_2 system mimics the reaction between particles in the lung and their reaction after being engulfed by macrophages in the lung.

Spin trapping was used to detect short-lived free radical intermediates. This technique involved the addition-type reaction of a short-lived radical with a paramagnetic compound (spin trap) to form a relatively long-lived free radical product (spin adduct), which was then studied using conventional ESR. The radical generation potential of DWCNT was examined in the presence of H_2O_2 or H_2O_2 plus $FeSO_4$ (0.1 m*M*).

Animals

C57BL/6J male mice (7 wk old) were purchased from Jackson Laboratories (Bar Harbor, ME). Animals were housed in an AAALAC-accredited, specific-pathogen-free,

environmentally controlled facility and allowed to acclimate at least 7 d prior to use. Mice were monitored to be free of endogenous viral pathogens, parasites, mycoplasmas, *Helicobacter*, and CAR *Bacillus*. Mice were kept in ventilated cages, which were provided HEPA-filtered air, with Alpha-Dri virgin cellulose chips and hardwood Beta-chips for bedding. The animals were maintained on a Harlan Teklad 7913, 6% fat, irradiated diet and tap water, both of which were provided ad libitum. All animal protocols were approved by the NIOSH/Morgantown Institutional Animal Care and Use Committee.

Mouse Pharyngeal Aspiration

In order to prepare the DWCNT for pharyngeal aspiration, they were suspended in carboxymethylcellulose (CMC) at a concentration of 0.8 mg/ml. CMC was used as a dispersant to obtain a homogeneous suspension of DWCNT. Briefly, to suspend the Toray DWCNT, a stock of 0.3% (w/v) carboxymethylcellulose (CMC) was prepared. Specifically, 0.3 g CMC (Sigma-Aldrich catalogue number 419273) was mixed with 100 ml 0.9% NaCl (saline) solution. The CMC/saline solution was then mixed by mechanical stirring with low heat until the solution was clear (approximately 30–40 min). Once the CMC solution cooled to room temperature, 10 mg Toray DWCNT was added to 10 ml CMC solution. The CMC/DWCNT suspension was then sonicated on ice (Branson Sonifer 450, 25 W continuous output, 20 min). Next, the CMC/DWCNT combination underwent centrifugation to remove any large agglomerated masses from the suspension (10,000 $\times$ g, 15 min, 4°C). The supernatant was then aspirated and saved for further analysis and mice aspiration procedures. To verify the concentration of DWCNT in the solution, the absorbance of the aspirated supernatant at 500 nm was assessed. Utilizing the obtained absorbance, the DWCNT concentration was then calculated using molar absorptivity constant at 500 nm, which is $\varepsilon = 45$ (cm^2/mg). Once the concentration of the Toray DWCNT solution was determined, mice were exposed to 0, 1, 10, or 40 μg/mouse of DWCNT by pharyngeal aspiration as described by Rao et al. (2003).

Briefly, the animals were anesthetized with isoflurane and placed on a board in a near-vertical position. The animal's tongue was extended with lined forceps, and 50 μl of the respective particle suspension was placed on the back of the tongue, which was held until the suspension was aspirated into the lungs. Control mice were administered an equal volume of CMC. Mice were sacrificed 1, 7, or 56 d following aspiration exposure. These postexposure times were chosen to compare the bioactivity of the DWCNT to MWCNT used in previous studies from our lab (Porter et al., 2010).

Whole Lung Lavage

At 1, 7, and 56 d postexposure, mice were weighed and anesthetized with an intraperitoneal (ip) injection of sodium pentobarbital (>100 mg/kg) followed by euthanasia by exsanguination under deep anesthesia. The trachea was cannulated with a blunted 22-gauge needle, and whole-lung lavage (WLL) was performed using cold sterile Ca^{2+}- and Mg^{2+}-free phosphate-buffered saline (PBS) at a volume of 0.6 ml for first lavage (kept separate) and 1 ml for subsequent lavages. Approximately 4 ml WLL fluid per mouse was pooled and collected in sterile centrifuge tubes. Pooled WLL cells were washed in PBS by centrifugation (600 $\times$ g, 10 min, 4°C) and resuspended in PBS. Acellular first-fraction WLL aliquots were utilized for analysis of lactate dehydrogenase activity (LDH) and albumin levels.

Cell Counts and Differentials and First WLL Fluid Analyses

Total WLL cell counts were obtained using a Coulter Multisizer 3 (Coulter Electronics, Hialeah, FL), and cytospin preparations of the WLL cells were made using a cytocentrifuge (Shandon Elliot Cytocentrifuge, London, UK). The cytospin preparations were stained with

modified Wright–Giemsa stain, and cell differentials were determined by light microscopy. Lactate dehydrogenase (LDH) activities and albumin concentrations of the first WLL fluid were measured to assess cytotoxicity and the integrity of the lung blood–gas barrier, respectively. LDH activities and albumin concentrations were measured using a COBAS MIRA Plus chemical analyzer (Roche Diagnostic Systems, Inc., Montclair, NJ) as previously described (Porter et al., 2010).

Enhanced Dark-Field Microscopy

The enhanced dark-field images taken using the CytoViva microscope at 56 d postexposure allowed for determination of where the Toray DWCNT are found within the lung. Mice (male, C57BL/6J, 7 wk old) were dosed with 40 μg/mouse of the specific Toray DWCNT suspensions following the same procedures outlined earlier. At 56 d postexposure, mice were anesthetized with an intraperitoneal injection of sodium pentobarbital (>100 mg/kg body weight, ip), followed by euthanasia by transection of the abdominal aorta. Lungs were rapidly removed and fixed by intratracheal perfusion with 1 ml of 10% neutral buffered formalin. Lungs were then processed overnight in a tissue processor and embedded in paraffin. Sections (5 μm thick) were collected on precleaned slides, deparaffinized, and stained with Sirius red before being cover-slipped. Slides were imaged using a high signal-to-noise, dark-field-based illumination on a CytoViva Olympus BX-41 microscope (CytoViva, Auburn, AL) at 100× with oil immersion. Images of the lung tissue were captured with a Dage MTI digital camera (2048×2048, Dage, Michigan City, IN).

Field Emission Scanning Electron Microscopy

For field emission scanning electron microscopy, mice (male, C57BL/6J, 7 wk old) were dosed with 40 μg/mouse of the specific Toray DWCNT suspensions following the same procedures outlined earlier. At 56 d postexposure, mice were anesthetized with an intraperitoneal injection of sodium pentobarbital (>100 mg/kg body weight, ip), followed by euthanasia by transection of the abdominal aorta. Lungs were rapidly removed and fixed by intratracheal perfusion with 1 ml of 10% neutral buffered formalin. Lungs were then processed overnight in a tissue processor and embedded in paraffin. Sections of the lung were then cut at 8 μm, placed on carbon planchets, deparaffinized, and sputter-coated. After coating, the specimens were examined using a Hitachi model S-48-00 field emission scanning electron microscope (FESEM) (Hitachi High Technologies, Gaithersburg, MD) at 5 to 20 kV.

Histopathology

Lung histopathology was performed as previously described (Hubbs et al., 1997). Briefly, mice were anesthetized with an ip injection of sodium pentobarbital (>100 mg/kg), followed by euthanasia by exsanguination. Whole lungs were inflated with 1 ml of 10% neutral buffered formalin. All collected tissues were trimmed the same day, with sections of the right and left lung lobes, and the tracheobronchial lymph nodes, if found, were also trimmed. Tissues were processed overnight and embedded the following day in paraffin.

Lung sections (5 μm thick) were stained with hematoxylin and eosin (H&E), picrosirius red, and Masson's trichrome. All slides were interpreted blindly by a board-certified veterinary pathologist. Microscopic evaluation included assessments of inflammation and fibrosis in the lung and particle translocation to the tracheobronchial lymph node (TBL). Each histopathologic change was scored for distribution and for severity according to the following parameters: distribution (0 = none, 1= focal, 2 = focally extensive, 3 = multifocal, 4 = multifocal and coalescent, 5 = diffuse) and severity scores (0 = none, 1 = minimal, 2 = mild, 3 = moderate, 4 = marked, 5 = severe) as previously described by Hubbs et al. (1997). A composite score for each change consisting of the sum of the distribution and severity scores

were recorded. All diagnoses were recorded electronically in the PathData recording system (PDS Pathology Data System Ltd., Switzerland) and tabulated by animal. Additionally, mean composite scores were calculated from the mean distribution and severity scores for each group.

Statistics

Statistical comparisons between doses of DWCNT at a specific postexposure time were performed separately for each postexposure time using analysis of variance (ANOVA) with post hoc *t*-tests for pair-wise comparison of dose groups. Similar analyses were performed to compare postexposure time effect for each exposure group. Since variance estimates were different across dose groups, the ANOVA models were estimated using an unequal variance model available from SAS PROC MIXED. All statistical tests were two-tailed with significance level equal to .05.

Since the pathology data consisted of ordinal scores rather than comparisons between control and DWCNT-exposed mice at each time, comparisons across time for each exposure group were accomplished using two separate one-way nonparametric analyses of variance (ANOVA). Exact tests were used because of the high number of tied values in the data. The nonparametric ANOVA was performed using SAS Proc NPAR1WAY with exact Kruskal–Wallace tests for multigroup comparisons and exact Wilcoxon tests for post hoc pairwise comparisons. All statistical tests were two-tailed and performed at the .05 significance level.

RESULTS

Trace Metal Analysis

The trace metal analysis of the bulk DWCNT sample revealed that Toray DWCNT trace metal contamination was 0.83%, with iron (Fe) (0.58%) and chromium (Cr) (0.21%) being the two major metal contaminants. The trace metal analyses revealed that no other metal contaminants were present above 0.02%.

Electron Spin Resonance Studies

The potential of Toray DWCNT to generate free radicals was measured using electron spin resonance (ESR) and DMPO as a spin trap. The results in Figure 1 show radicals generated when reacting DWCNT with H_2O_2 using the classic Fenton reaction:

$$H_2O_2 + Fe^{2+} \rightarrow {}^{\bullet}OH + OH^- + Fe^{3+}$$

Figure 1 (A and B) shows the Fenton reaction and generated $^{\bullet}OH$ radicals in PBS and in the CMC dispersion media, respectively, showing that the CMC dispersion media exerted no significant effect on the DMPO trapping of $^{\bullet}OH$ radicals. As previously mentioned, CMC was used as a dispersant to obtain a homogeneous suspension of DWCNT. When DWCNT were substituted for Fe when reacting with H_2O_2 there were no measurable radicals generated (Figure 1C), suggesting that DWCNT have no available transition metals to react with H_2O_2 and generate $^{\bullet}OH$. This further suggests that DWCNT cannot act in a Fenton-like manner themselves and generate $^{\bullet}OH$ radicals. The combination of DWCNT and $FeSO_4$ (Figure 1D) showed some measurable radicals, but at significantly lower amounts than $FeSO_4$ by itself. These observations imply that DWCNT are acting as scavengers or exerting a quenching effect on $^{\bullet}OH$ radicals similar to fullerenes (Krusic et al., 1991) and other forms of CNT (Fenoglio et al., 2006; Tsuruoka et al., 2012). It is possible that DWCNT exposure may stimulate the cells to generate hydrogen peroxide and superoxide radicals via activation of NADPH oxidase. However, this mechanism is not fully understood but may be associated with high electron affinity of the carbon atoms in the nanotube framework. In turn, these reactive oxygen species (ROS) may be the driving force to produce lung injury.

Comparison of Pulmonary Inflammation and Damage of DWCNT Exposures

At 1 d postexposure, Toray DWCNT produced a significant, dose dependent increase in polymorphonuclear leukocyte (PMN) counts

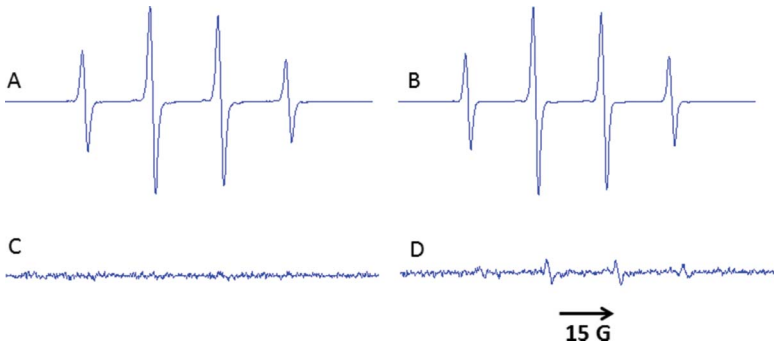

FIGURE 1. ESR spectra of radicals generated from Toray DWCNT exposures. (A) PBS, DMPO (100 m*M*), H_2O_2 (1 m*M*), and $FeSO_4$ (0.1 m*M*); (B) CMC, DMPO (100 m*M*), H_2O_2 (1 m*M*), and $FeSO_4$ (0.1 m*M*); (C) CMC, DMPO (100 m*M*), H_2O_2 (1 m*M*), and Toray DWCNT (27 mg/ml); (D) CMC, DMPO (100 m*M*), H_2O_2 (1 m*M*), Toray DWCNT (27 mg/ml), and $FeSO_4$ (0.1 m*M*). Panels A and B are at 30× scale to panels C and D. All spectra were run using these settings: center field 3470 G, sweep width 100 G, microwave frequency 9.749 GHz, microwave power 63 mW, and time constant 40.960 ms (color figure available online).

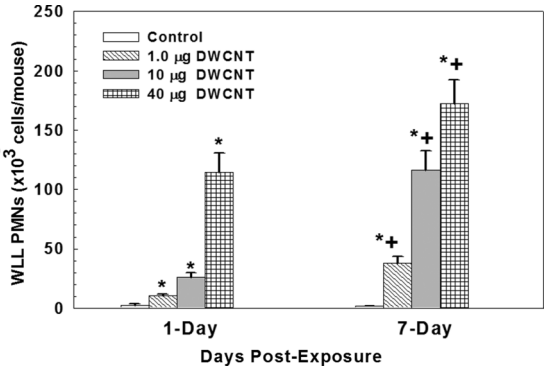

FIGURE 2. Comparison of inflammation induced by pharyngeal aspiration exposure to 0, 1, 10, or 40 μg/mouse of Toray DWCNT at 1 and 7 d postexposure. WLL PMN were used as a marker of pulmonary inflammation. Values are given as means ± SE ($n = 8$). An asterisk indicates that PMN influx for that group was significantly higher than control ($p < .05$). A plus mark (+) indicates that PMN influx was significantly different between groups at an equivalent mass dose at different postexposure time points ($p < .05$).

in WLL samples over control (Figure 2). The pulmonary inflammation, as indicated by PMN influx, also exhibited a dose-dependent rise at 7 d postexposure (Figure 2). The results demonstrate that not only were PMN counts significantly higher than control levels, but PMN influx at 7 d postexposure was significantly higher at all doses when compared to PMN counts at 1 d postexposure.

LDH activities were measured in the first fraction of the WWL fluid to assess cytotoxicity after Toray DWCNT exposure. Similar to the PMN influx, DWCNT exposure produced a dose-dependent elevation in LDH activities in the WLL fluid at both 1 and 7 d postexposure (Figure 3). LDH activities at the highest dose (40 μg/mouse) at 7 d postexposure resulted in significantly greater cell damage compared to the same dose at 1 d postexposure. In contrast, at 7 d postexposure the low and intermediate doses (1 and 10 μg/mouse) of DWCNT produced a significant increase in LDH activity over control but the rise was not significantly higher than LDH activities at 1 d postexposure groups at the same doses (Figure 3).

Albumin levels in the first fraction of WLL fluid were analyzed to assess air/blood barrier injury after Toray DWCNT exposure. At both 1 and 7 d postexposure, DWCNT exposure produced a dose-dependent elevation in albumin levels. At 1 and 7 d postexposure, a significant increase in albumin levels above control was found at all doses of DWCNT exposure (Figure 4). However, no significant differences existed between albumin levels of the 1 and 7 d postexposure groups of the same dose.

Enhanced Dark-Field Microscopy Imaging

The enhanced dark-field images taken using the CytoViva microscope at 56 d postexposure allowed for determination of where the Toray DWCNT are found within the lung. The results of the CytoViva microscopy studies indicate that DWCNT are observed to

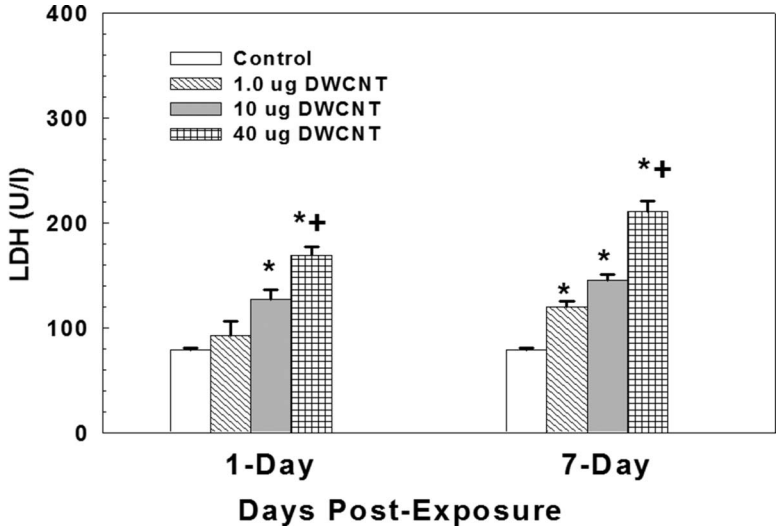

FIGURE 3. Comparison of cytotoxicity induced by pharyngeal aspiration exposure to 0, 1, 10, or 40 μg/mouse of Toray DWCNT at 1 and 7 d postexposure. WLL fluid LDH activities were used as a marker of cytotoxicity. Values are given as means ± SE ($n = 8$). An asterisk indicates that LDH activity for that group was significantly higher than control ($p < .05$). A plus mark (+) indicates that cytotoxicity was significantly different between groups at an equivalent mass dose at different postexposure time points ($p < .05$).

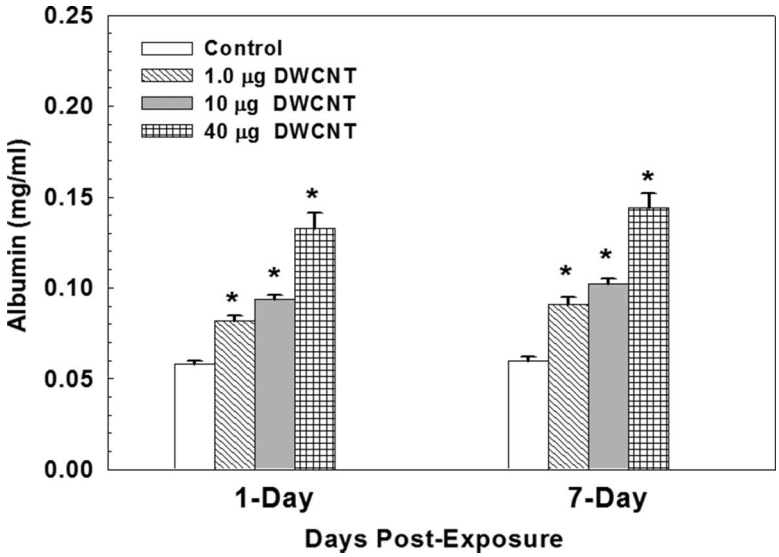

FIGURE 4. Comparison of air/blood barrier injury induced by pharyngeal aspiration exposure to 0, 1, 10, or 40 μg/mouse of Toray DWCNT at 1 and 7 d postexposure. WLL fluid albumin concentrations were used as a marker of air/blood barrier damage. Values are given as means ± SE ($n = 8$). An asterisk indicates that albumin levels for that group were significantly higher than control ($p < .05$).

be generally diffuse within the interstitial tissue, but also in condensed areas of alveolar macrophages (Figure 5).

Field Emission Scanning Electron Microscopy

The FESEM micrograph (Figure 6) supports the prior enhanced dark-field microscopy-based observations that at 56 d postexposure the Toray DWCNT are found within the lung. The FESEM micrograph demonstrates the presence of both agglomerated and singlet Toray DWCNT within the interstitial tissue of the exposed animals at 56 d postexposure.

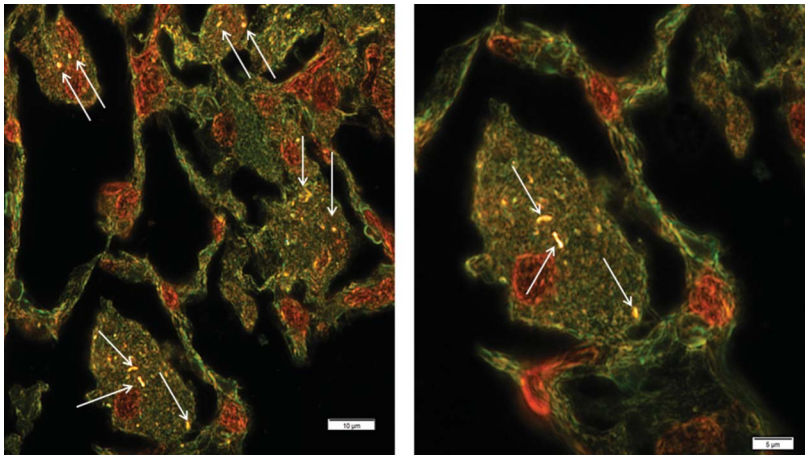

FIGURE 5. Enhanced dark-field image from a 56-d postexposure lung showing Toray DWCNT fibers. Toray DWCNT fibers are brightly expressed in enhanced dark-field images due to the scattering of light, while tissues are dark and airspaces are black. The arrows indicate the presence of Toray DWCNT within alveolar macrophages (color figure available online).

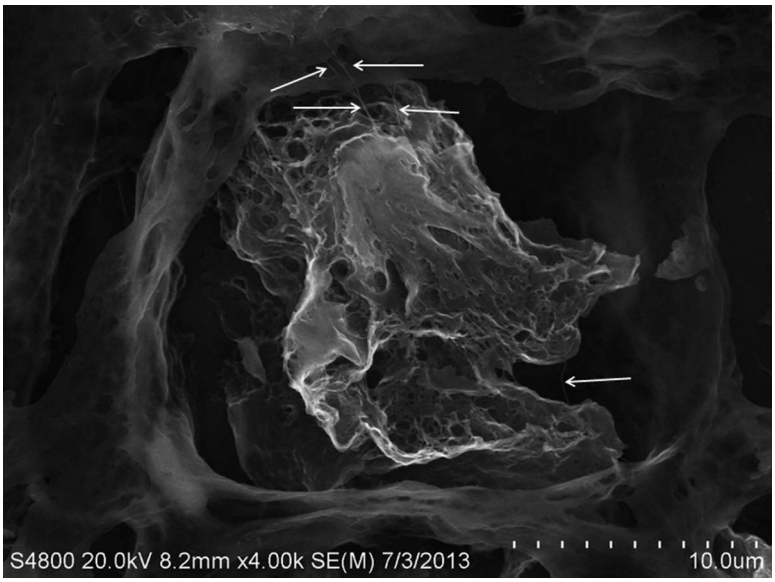

FIGURE 6. Field emission scanning electron micrograph from the lung of a mouse 56 d after a single, 40-μg/mouse aspiration exposure to Toray DWCNT. The lung tissue was examined using a Hitachi model S-48-00 field emission scanning electron microscope (FESEM) (Hitachi High Technologies, Gaithersburg, MD) at 5 to 20 kV. The arrows indicate the presence of Toray DWCNT within interstitial tissue of the mouse lung.

Histopathological Analyses

Lung—7 d Postexposure The histopathological findings are presented in Table 1. In mice of the d-7 sacrifice, analyses indicated the presence of phagocytosed foreign material in the lung. Specifically, at 7 d postexposure, the presence of this phagocytosed foreign material was noted in and significantly elevated in all animals exposed to Toray DWCNT compared to control. The increase in severity in this finding was related to the dose level. Most often, the material was phagocytosed by macrophages and multinucleated giant cells. However, some DWCNT were also detected free within the alveolar space.

In addition, other histopathology findings in the lungs at 7 d postexposure included alveolitis (nonmacrophage leukocytic infiltrates

within alveolar lumina) and interstitial fibrosis (thickening of alveolar septae with increased collagen formation). Alveolitis consisted of minimal to moderate numbers of macrophages and neutrophils that expanded the alveolar septa and filled the alveolar space. With the lowest dose (1 μg/mouse) alveolitis was not evident. However, a dose-dependent increase in alveolitis existed for the intermediate and high doses (10 and 40 μg/mouse, respectively) of DWCNT. There was also a dose-dependent rise in incidence of fibrosis. At the lowest dose (1 μg/mouse), fibrosis was not evident. However, a dose-dependent elevation in fibrosis existed for the intermediate and high doses (10 and 40 μg/mouse, respectively) of DWCNT. In fact, at the intermediate dose 50% of treated animals developed fibrosis, while at the highest dose (40 μg/mouse) 100% developed fibrosis.

Lung—56 d Postexposure At 56 d postexposure, similar to the 7-d postexposure group, the analyses indicated the presence of phagocytosed foreign material in the lung. Furthermore, the prevalence and severity of alveolitis were present but reduced compared to the 7 d postexposure group (Figure 7). In addition, the presence of interstitial fibrosis at 56 d postexposure was similar to the fibrotic response observed in the 7-d postexposure group (Table 2). In fact, as with the 7-d postexposure group, there was a dose-dependent increase in the presence of fibrosis. No fibrosis was present at the lowest (1 μg/mouse) dose. However, at the intermediate and high doses (10 and 40 μg/mouse) the development of fibrosis was noted. As with the 40-μg/mouse dose at 7 d postexposure, 100% of animals receiving the 40-μg/mouse dose at 56 d postexposure developed fibrosis (Figure 7 and Table 2).

Tracheobronchial Lymph Node (TBL)—7 d Postexposure The only clear treatment-related finding in the TBL was the presence of phagocytosed foreign material, which occurred in animals exposed to the highest dose (40 μg/mouse) of DWCNT. The foreign material, which was virtually identical to foreign material in the lung, was present within the cytoplasm of macrophages that were scattered primarily throughout the paracortex and medulla. The severity of this finding was minimal in all affected TBL.

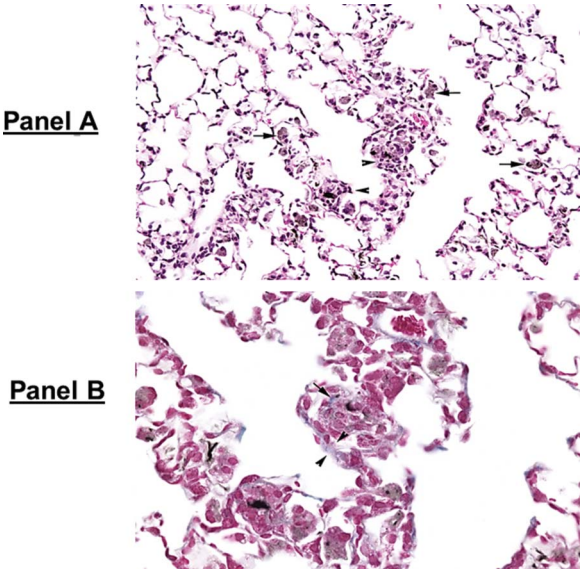

FIGURE 7. (A) Photomicrograph (200×) from the lung of a mouse 56 d after a single aspiration exposure to Toray DWCNT (40 μg/mouse). Mild alveolar space expansion was associated with interstitial Toray DWCNT. The inflammation is composed of foci of macrophages and lymphocytes (arrowheads). There are also numerous alveolar macrophages that contain abundant foreign material (arrows). (B) Photomicrograph at higher magnification (400×) of the same lung seen in (A). Trichrome stain highlights area of fibrosis. Arrowheads highlight thickening of the alveolar septa with increased blue staining (fibrosis). Within an area of inflammation that fills the alveolus there is a focus of fibrosis (arrow) (color figure available online).

Tracheobronchial Lymph Node—56 d Postexposure In mice sacrificed on d 56, the sole treatment-related finding in the TBL was the presence of phagocytosed foreign material, which increased in prevalence and severity when compared to 7-d postexposure groups. Mean severity scores for this finding were numerically higher for d-56 mice as compared to d-7 mice. Similar to d-7 mice, the generally low prevalence and severity of hemosiderin-laden macrophages in TBL subscapular sinuses of d-56 mice were comparable among control and treated mice.

DISCUSSION

Carbon nanotubes possess a wide range of possible applications in numerous sectors of

TABLE 2. Summary of Histopathological Findings

Postexposure (d)	Treatment	Total (*n*)	Alveolitis	Histiocytic aveolitis	Fibrosis	Phagocytosed nanoparticles
7	Control	8	0 ($n = 8$)	0 ($n = 8$)	0 ($n = 8$)	0 ($n = 8$)
	1.0 μg DWCNT	8	0 ($n = 8$)	0 ($n = 8$)	0 ($n = 8$)	4 ($n = 8$)*
	10 μg DWCNT	8	0 ($n = 5$)* 2 ($n = 2$) 3 ($n = 1$)	0 ($n = 4$)* 4 ($n = 4$)	0 ($n = 4$)* 3 ($n = 3$) 4 ($n = 1$)	5 ($n = 8$)*
	40 μg DWCNT	8	4 ($n = 2$)* 5 ($n = 6$)	4 ($n = 4$)* 5 ($n = 4$)	3 ($n = 1$)* 4 ($n = 7$)	5 ($n = 8$)*
56	Control	8	0 ($n = 8$)	0 ($n = 8$)	0 ($n = 8$)	0 ($n = 8$)
	1.0 μg DWCNT	8	0 ($n = 8$)	0 ($n = 8$)	0 ($n = 8$)	4 ($n = 8$)*
	10 μg DWCNT	8	0 ($n = 7$) 2 ($n = 1$)	1 ($n = 4$)* 4 ($n = 4$)	0 ($n = 6$) 3 ($n = 1$) 4 ($n = 1$)	5 ($n = 8$)*
	40 μg DWCNT	8	4 ($n = 2$)* 5 ($n = 6$)	4 ($n = 1$)* 5 ($n = 7$)	3 ($n = 2$)* 4 ($n = 6$)	4 ($n = 3$)* 5 ($n = 5$)

Note. Values represent histopathology score and inside parentheses the number of animals (*n*) with that score. Asterisk indicates significant difference between control and DWCNT group at the same postexposure time.

industry. Due to structural similarities in terms of their high aspect ratio (ratio of length to width), low dissolution, and biopersistence, it was postulated that CNT may exhibit toxic properties similar to those of other fibrous materials such as asbestos (Donaldson et al., 2006). Indeed, numerous in vivo studies have already demonstrated that both the single-walled and multiwalled varieties of the CNT, when instilled into the lungs of rodents, have the potential to produce inflammation, fibrosis (scarring of the lungs), and granuloma (small nodule) formation in the lung tissue (Lam et al., 2004; Muller et al., 2005; Shvedova et al., 2005; Chou et al., 2008; Porter et al., 2010; Murray et al., 2012; Guo et al., 2012; Sager et al., 2013).

The double-walled variety of the carbon nanotube family is a relatively new and unstudied variety of CNT. The DWCNT are coaxial nanostructures composed of exactly two single-walled carbon nanotubes, one nested in another (Shen et al., 2011). The unique inner-wall coupling structure of the DWCNT offers advantages for extending their applications. Due to their versatility and durability, their utilization is expected to continue to increase in the future. However, the exploration of possible adverse effects on human health has lagged behind their production and utilization. As previously mentioned, recent studies demonstrated that MWCNT and SWCNT induce a severe inflammatory and fibrotic response (Porter et al., 2010; Sager et al., 2013; Murray et al., 2012). However, in vivo pulmonary toxicity studies examining other varieties of CNT, such as the DWCNT, have not been adequately addressed. In this study, the capacity of DWCNT exposure to facilitate a proinflammatory and profibrotic pulmonary response was investigated.

Comparison of Cytotoxic Response of MWCNT and DWCNT

The current study results show that pulmonary exposure to DWCNT facilitated a significant cytotoxic, inflammatory pulmonary response, hallmarked by an influx of PMN, an increase in LDH activity, and elevation in albumin levels at both 1 and 7 d postexposure. In comparing these results to similar MWCNT studies recently conducted by our lab (Sager et al., 2013), the PMN influx generated by DWCNT at 1 d postexposure was lower than the PMN influx produced by the same mass dose of MWCNT. However, with the MWCNT exposure, PMN influx was transient and markedly reduced at 7 d postexposure, but with the DWCNT, PMN influx continued to rise

significantly from 1 d to 7 d postexposure for all doses. In fact, at 7 d postexposure, PMN influx facilitated by the DWCNT was greater than the PMN influx produced by the MWCNT.

DWCNT exposure also induced a dose-dependent increase in LDH activity in lung lavage fluid at both 1 and 7 d postexposure. In comparison to our MWCNT data, LDH activity induced by MWCNT was initially higher at 1 d postexposure than LDH activity levels produced by similar doses of DWCNT at 1 d postexposure. However, as with PMN influx, MWCNT exposure produced a transient, significant increase in LDH activity, which declined significantly at 7 d postexposure. With the DWCNT exposure, LDH activity at 1 d postexposure was significantly elevated over control, at all doses, and unlike for the MWCNT, DWCNT LDH activity levels continued to rise at 7 d postexposure.

DWCNT exposure also produced a dose-dependent increase in albumin levels at both the 1- and 7-d postexposure time points. When comparing 1 and 7 d postexposure, the air–blood barrier injury induced by exposure to the DWCNT remained constant from 1 to 7 d postexposure. In comparison to our MWCNT data, albumin levels produced by MWCNT were similar at 1 d postexposure when compared to albumin levels produced by the DWCNT at 1 d postexposure. However, at 7 d postexposure MWCNT albumin levels significantly declined, while the DWCNT albumin levels remained nearly the same as the 1-d postexposure levels.

The trend of the inflammatory and cytotoxic responses produced by DWCNT exposure was also reflected in the histopathological findings. In comparison to the MWCNT histopathologic studies that our lab recently conducted (Sager et al., 2013), the 40-μg/mouse dose of DWCNT produced a greater degree of alveolitis and fibrosis than the 40-μg/mouse dose of MWCNT at both 7 and 56 d postexposure. Specifically, at 7 d postexposure 50% of the animals treated with MWCNT presented with mild alveolitis, while 100% of the animals treated with DWCNT were found to display moderate alveolitis. For fibrosis, at 7 d postexposure, histopathological findings showed that 37% of the animals treated with MWCNT possessed mild fibrosis, while 100% of the animals treated with DWCNT developed moderate fibrosis. At 56 d postexposure, histopathologic findings revealed that 63% of the animals treated with MWCNT were found to display mild alveolitis, while 100% of the animals treated with DWCNT were found to present with moderate alveolitis. Further, histopathologic analysis showed that in regard to fibrosis at 56 d postexposure, 60% of the animals treated with MWCNT were found to display mild fibrosis, while 100% of the animals treated with DWCNT were found to present with moderate fibrosis.

Probable DWCNT Cytotoxic Mechanisms

It has been widely hypothesized that toxic nanoparticles may potentially increase phagolysosomal membrane permeability and release of cathepsin B. In turn, cathepsin B release facilitates the activation of the NLRP3 inflammasome. The activation of the NLRP3 inflammasome induces the release of pro-inflammatory cytokines (such as IL-1β and IL-18) from alveolar macrophages (AM) and most likely IL-33 from epithelial cells (Beamer et al., 2012). This family of proinflammatory cytokines was reported to significantly contribute to acute inflammatory responses such as PMN infiltration (Hamilton et al., 2009) and fibrosis (Wang et al., 2012) both in vitro and in vivo.

More specifically, when inhaled particles, including DWCNT, deposit in the distal airways and alveoli, they are likely engulfed by AM (Bals et al., 1999). During the phagocytosis process, the inhaled particles are taken up into the macrophage phagolysosomes. This uptake of the inhaled particle into the phagolysosome catalyzes damage, phagolysosome leakage, and cathepsin B release. This initial release of cathepsin B from the phagolysosomes initiates the activation of the NLRP3 inflammasome, which leads to the release of IL-1β, IL-18, and IL-33. These cytokines are secreted into the alveolar lining fluid of the lung and

in turn work synergistically to promote inflammation and fibrosis in the lung (Cassel et al., 2009).

In support of this theory, our lab demonstrated that NLRP3 inflammasome activation is potentially the driving force behind both the inflammatory response and fibrogenic response of MWCNT exposure (Sager et al., 2013). The findings of our previous study suggested that the NLRP3 inflammasome was activated in vivo, after pulmonary exposure to MWCNT. Our data support the notion that the NLRP3 inflammasome plays a crucial role in the pathogenic response to MWCNT. In fact, data from the previous study supported a relationship between the extent of NLRP3 inflammasome activation and degree of pulmonary inflammation and fibrosis. Further, evidence provided from the previous MWCNT study indicated that activation of the NLRP3 inflammasome is a reliable indicator of lung pathogenesis. In fact, many recent therapeutic goals to treat chronic inflammation in the lung have focused on interrupting or blocking the NLRP3 inflammasome pathway (Arend et al., 2008). Therefore, future studies exploring the role of the NLRP3 inflammasome in DWCNT lung pathogenesis would be of great interest.

In agreement with our lab's previous studies, this study is a part of a larger program with the end goal of determining how various physicochemical properties of different varieties of CNT influence their pathogenicity. Specifically, DWCNT assessed in this study facilitated a robust inflammatory and fibrotic response. When compared to the other varieties of CNT, DWCNT would tend to be less bioactive in the lung than SWCNT (Shvedova et al., 2005; Murray et al., 2012) but more bioactive in the lung than the MWCNT (Sager et al., 2012). In the future, such information on the differing varieties of CNT may allow material scientists to incorporate a "safety by design" philosophy into the development of new nanoparticle-based technologies, which would in turn synthesize and use nanomaterials that pose lower risks to human health.

REFERENCES

Abuilaiwi, F., Laoui, T., Al-Harthi, M., and Atieh, M. A. 2010. Modification and functionalization of multiwalled carbon nanotube (MWCNT) via Fischer esterification. *Arab. Sci. Eng*. 35(1C).

Arend, W., Palmer, G., and Gagay, C. 2008. IL-1, IL-18, and IL-33 families of cytokines. *Immunol. Rev*. 223: 20–38.

Bals, R., Weiner, D., and Wilson, J. 1999. The innate immune system in cystic fibrosis lung disease. *J. Clin. Invest*. 103: 303–307.

Beamer, C. A., Girtsman, T. A., Seaver, B. P., Finsaas, K. J., Migliaccio, C. T., Perry, V. K., Rottman, J. B., Smith, D. E., and Holian, A. 2013. IL-33 mediates mutli-walled carbon nanotube (MWCNT)-induced airway hyper-reactivity via the mobilization of innate helper cells in the lung. *Nanotoxicology* [Epub ahead of print, June 29].

Bergamaschi, E. 2009. Occupational exposure to nanomaterials: Present knowledge and future development. *Nanotoxicology* 3: 194–201.

Cassel, S., Eisenbarth, S., Iyer, S., Sadler, J., Colegio, O., Tephly, L., Carter, A., Rothman, P., Flavell, R., and Sutterwala, F. 2009. The Nalp3 inflammasome: a sensor of immune danger signals. *Semin. Immunol*. 21: 194–198.

Chou, C.-C., Hsiao, H.-Y., Hong, Q.-S., Chen, C.-H., Peng, Y.-W., Chen, H.-W., and Yang, P.-C. 2008. Single-walled carbon nanotubes induce pulmonary injury in mouse model. *Nano Lett*. 8: 437–445.

Crouizer, D., Follot, S., Gentilhomme, E., Flahaut, E., Arnaud, R., Dabouis, V., Castellarin, C., and Debouzy, J. 2010. Carbon nanotubes induced inflammation but decrease the production of reactive oxygen species in lung. *Toxicology* 272: 39–45.

Dresselhaus, M., Dresselhaus, G., and Avouris, P. 2001. *Carbon nanotubes: Synthesis, structure, properties, and applications*. Heidelberg, Germany: Springer-Verlag.

Donaldson, K., Aitken, R., Tran, L., Stone, V., Duffin, R., Forrest, G., and Alexander,

A. 2006. Carbon nanotubes: A review of their properties in relation to pulmonary toxicology and workplace safety. *Toxicol. Sci*. 92: 5–22.

Donaldson, K., Murphy, F. A., Duffin, R., and Poland, C. A. 2010. Asbestos, carbon nanotubes and the pleural mesothelium: A review of the hypothesis regarding the role of long fibre retention in the parietal pleura, inflammation and mesothelioma. *Particle Fibre Toxicol*. 7: 5–16.

Fenoglio, I., Tomatis, M., Lison, D., Muller, J., Fonseca, A., Nagy, J. B., and Fubini, B. 2006. Reactivity of carbon nanotubes: Free radical generation or scavenging activity? *Free Radical Biol. Med*. 40: 1227–1233.

Guo, N., Wan, Y., Denvir, J., Porter, D., Pacurari, M., Wolfarth, M., Castranova, V., and Qian, Y. 2012. Multiwalled carbon nanotube-induced gene signatures in the mouse lung: Potential predictive value for human lung cancer risk and prognosis. *J. Toxicol. Environ. Health A* 75: 1129–1153.

Hamilton, Jr., R., Wu, N., Porter, D., Buford, M., Wolfarth, M., and Holian, A. 2009. Particle length-dependent titanium dioxide nanomaterials' toxicity and bioactivity. *Particle Fibre Toxicol*. 6: 35–41.

Hubbs, A. F., Castanova, V., Ma, J. Y. C., Frazer, D. G., Siegel, P. D., Ducatman, B. S., Grote, A., Schwegler-Berry, D., Robinson, V. A., VanDyke, C., Barger, M., Xiang, J., and Parker. J. 1997. Acute lung injury induced by a commercial leather conditioner. *Toxicol. Appl. Pharmacol*. 143: 37–46

Jaurand, M., Renier, A. and Daubriac, J. 2009. Mesothelioma: Do asbestos and carbon nanotubes pose the same health risk? *Particle Fibre Toxicol*. 6: 16–20.

Jorio, A., Dresselhaus, M., and Dresselhaus, G. 2008. Potential applications of carbon nanotubes. In *Topics in applied physics*, vol. 11, 13–613. Berlin, Germany: Springer-Verlag.

Kim, J. K., Song, K. S., Joo, H. J., Lee, J. H. and Yu, I. J. 2010. Determination of cytotoxicity attributed to multiwall carbon nanotubes (MWCNT) in normal human embryonic lung cell (WI-38) line. *J. Toxicol. Environ. Health A* 73: 1521–1529.

Krusic, P. J., Wasserman, E., Keizer, P. N., Morton, J. R., and Preston, K. F. 1991. Radical reaction of C60. *Science* 254: 1183–1185.

Lam, C.-W., James, J. T., McCluskey, R., and Hunter, R. L. 2004. Pulmonary toxicity of single-wall carbon nanotubes in mice 7 and 90 days after intratracheal instillation. *Toxicol. Sci*. 77: 126–134.

Leonard, S., Roberts, J., Antonini, J., Castranova, V., and Shi, X. 2004. PbCrO4 mediates cellular responses via reactive oxygen species. *Mol. Cell. Biochem*. 255: 171–179.

Manke, A., Wang, L., and Rojanasakul, Y. 2012. Pulmonary toxicity and fibrogenic response of carbon nanotubes. *Toxicol. Mech. Methods* [Epub ahead of print].

Maynard, A. D., Baron, P. A., Foley, M., Shvedova, A. A., Kisin, E. R., and Castranova, V. 2004. Exposure to carbon nanotube material: Aerosol release during the handling of unrefined single-walled carbon nanotube material. *J. Toxicol. Environ. Health A* 67: 87–107.

Meunier, B., Coste, A., Olagnier, D., Authier, H., Lefevre, L., Dardenne, C., Bernad, J., Beraud, M., Flahaut, E., and Pipy, B. 2012. Double-walled carbon nanotubes trigger IL-1β release in human monocytes through Nlrp3 inflammasome activation. *Nanomedicine* 8: 987–995.

Muller, J., Huaux, F., Moreau, N., Mission, P., Heilier, J. F., and Delos, M. 2005. Respiratory toxicity of multi-wall carbon nanotubes. *Toxicol. Appl. Pharmacol*. 207: 221–231.

Murray, A., Kisin, E., Tkach, A., Yanamala, N., Mercer, R., Young, S., Fadeel, B., Kagan, V. M., and Shvedova, A. 2012. Factoring-in agglomeration of carbon nanotubes and nanofibers for better predicition of their toxicity versus asbestos. *Particle Fibre Toxicol*. 9: 10.

Musee, N., Thwala, M., and Nota, N. 2011. The antibacterial effects of engineered nanomaterials: Implications for wastewater treatment plants. *J. Environ. Monitor*. 13: 1164–1170.

Nagai, H., Okazaki, Y., Chew, S. H., Misawa, N., Yamashita, Y., Akatsuka, S., Ishihara, T., Yamashita, K., Yoshikawa, Y., Yasui, H., Jiang, L., Ohara, H., Takahashi, T., Ichihara, G.,

Kostarelos, K., Miyata, Y., Shinohara, H., and Toyokuni, S. 2011. Diameter and rigidity of multiwalled carbon nanotubes are critical factors in mesothelial injury and carcinogenesis. *Proc. Natl. Acad. Sci. USA* 108: E1330–E1338.

Patel, V. 2011. Global carbon nanotubes market outlook: Industry beckons. *Nanotech Insights* 2: 31–35.

Porter, D. W., Hubbs, A., Mercer, R., Wu, N., Wolfarth, M., Sriram, K., Leonard, S., Battelli, L., Schwegler-Berry, D., Friend, S., Andrew, M., Chen, B. T., Tsuroka, S., Endo, M., and Castranova, V. 2010. Mouse pulmonary dose and time course-responses induced by exposure to multi-walled carbon-nanotubes. *Toxicology* 269: 136–147.

Rao, G., Tinkle, S., Weissman, D., Antonini, J., Kashon, M., Salmen, R., Battelli, L., Willard, P., Hoover, M., and Hubbs, A. 2003. Efficacy of a technique for exposing the mouse lung to particles aspirated from the pharynx. *J. Toxicol. Environ. Health A* 66: 1441–1452.

Sager, T., Wolfarth, M., Friend, S., Hubbs, A., Hamiliton, R., Wu, N., Yang, F., Porter, D., and Holian, A. 2013. Effect of multi-walled carbon nanotube surface modification on bioactivity and inflammasome activation in the C57Bl/6 mouse model. *Nanotoxicology*, in press.

Shen, C., Brozena, A., and Wang, Y. 2011. Double-walled carbon nanotubes: Challenges and opportunities. *Nanoscale* 3: 503–518.

Shvedova, A., Kisin, R., Mercer, R., Murray, R., Johnson, V., Potapovich, A., Tyurina, Y., Gorelik, O., Arepalli, S., Schwegler-Berry, D., Hubbs, A., Antonini, J., Evans, D., Ku, B., Ramsey, D., Maynard, A., Kagan, V., Castranova, V., and Baron P. 2005. Unusual inflammatory and fibrogenic pulmonary responses to single-walled carbon nanotubes in mice. *Lung Cell. Mol. Physiol.* 289: L698–L708.

Stella, G. 2011. Carbon nanotubes and pleural damage: Perspectives of nanosafety in the light of asbestos experience. *Biointerphases* 2: P1–P17.

Tabet, L., Bussy, C., Amara, N., Setyan, A., Grodet, A., Rossi, M. J., Pairon, J. C., Boczkowski, J., and Lanone, S. 2009. Adverse effectsv of industrial multiwalled carbon nanotubes on human pulmonary cells. *J. Toxicol. Environ. Health A* 72: 60–73.

Tsuruoka, S., Takeuchi, K., Koyama, K., Noguchi, T., Endo, M., Tristan, F., Terrones, M., Matsumoto, H., Saito, N., Usui, Y., Porter, D., and Castranova, V. 2012. ROS evaluation for as eries of CNTs and their derivaties using the ESR method with DMPL. J. *Phys. Conf. Ser. Nanosafety*, in press.

Wang, X., Xia, T., Duch, M., Ji, Z., Zhang, H., Li, R., Sun, B., Lin, S., Meng, H., Liao, Y., Wang, M., Song, T., Yang, Y., Hersam, M., and Nel, A. 2012. Pluronic F108 coating decreases the lung fibrosis potential of multiwall carbon nanotubes by reducing lysosomal injury. *Nano Lett*. 12: 3050–3061.

Wang, L., Rojanasakul, Y., Castranova, V., Qiu, A., Lu, Y., Scabilloni, J., Wu, N., and Mercer, R. R. 2010. Direct fibrogenic effects of dispersed single-walled carbon nanotubes on human lung fibroblasts. *J. Toxicol. Environ. Health A* 73: 410–422.

Zhao, J., and Castranova, C. 2011. Toxicology of nanomaterials used in nanomedicine. *J. Toxicol. Environ. Health B* 14: 593–632.